



EARTH OBSERVATION AND GEOMATICS ENGINEERING

website: <https://eoge.ut.ac.ir>

Unsupervised change detection monitoring by feature change extraction using bi-temporal high resolution polarimetric SAR images

Sona Salehian Ghamsari , Hossein Arefi *, Reza Shah-Hosseini

School of Surveying and Geospatial Engineering, College of Engineering, University of Tehran, Tehran, Iran

Article history:

Received: 1 January 2020, Received in revised form: 1 May 2020, Accepted: 8 May 2020

ABSTRACT

Synthetic aperture radar (SAR) sensors are microwave active systems which represent a major tool for Earth observation. The completed information lying in the polarimetric channels represents a possibility for better detecting changes in different applications. In the literature, the log-ratio operator is applied to the original SAR image. In this paper, due to the use of full polarimetric images, first the coherency matrix, polarimetric decomposition, segmentation and data analysis features are extracted respectively, then the log-ratio and difference operators are applied to the extracted features. The use of decomposition increases the detection power due to extraction of single, double and volume bounce components. The aim of this work is proposing a framework for change detection in multi-temporal multi-polarization SAR data. In the novel representation, multi-temporal SAR images are employed to compute log-ratio polarimetric features. After pre-processing data, the coherency matrix, polarimetric decomposition, segmentation, and data analysis features are extracted. Then, the log-ratio and difference operators are applied to the features and create change maps using two unsupervised classification methods. The input of unsupervised classification is a stack of log-ratio features. Finally, the t_{1t_2} (changes from epoch1 to epoch 2) and t_{2t_1} (changes from epoch 2 to epoch 1) change maps, that are classification outputs, are fused. This representation is employed to design a novel unsupervised change detection approach for separating an unchanged class and two changed classes. The proposed approach is validated on a pair of UAVSAR data (L-band) acquired in Oakland, California, between the period 2010 to 2017. In the both groups of changes, the t_{1t_2} and t_{2t_1} , coherency based feature combination achieves the best result with an overall accuracy of 87% and Kappa of 74%. Considering all changes (both t_{1t_2} and t_{2t_1}), coherency based feature combination yields the best result with an overall accuracy of 86% and Kappa of 79%. As is clear from the evaluation results, the log-ratio operator has shown far better results among the two log-ratio and difference operators. However, the best option is the simultaneous use of the both operators so that the noise and error of the log-ratio operator can be reduced using the difference operator. According to the final results, it can be concluded that the coherence matrix is a better feature for detecting changes compared to other features.

KEYWORDS

Synthetic aperture radar (SAR)
Polarimetric SAR
Multi-temporal analysis
Change detection
Log-ratio decomposition feature
Unsupervised classification.

1. Introduction

Change detection is a process in remote sensing to identify changes. To identify land cover changes, two remote sensing images captured over the same geographical region and they are analyzed at different dates (Sharma & Mathur, 2004). Synthetic aperture radar (SAR) is a dependable and valuable data to obtain change information.

SAR imaging is of great benefit when it comes to undesirable weather conditions. It can be used properly under almost any atmospheric conditions (Ulaby et al., 1986; Al-Sharif et al., 2013). There is a direct link between the decomposition algorithm and the effectiveness and consistency of change detection, the results of change detection are determined by the status of decomposition

* Corresponding author

E-mail addresses: salehian.sona@ut.ac.ir (S. Salehian Ghamsari); hossein.arefi@ut.ac.ir (H. Arefi); rshahosseini@alumni.ut.ac.ir (R. Shah-Hosseini)

DOI: 10.22059/eoge.2020.299835.1078

(Schmitt & Brisco, 2013). Over the past few years, in order to obtain information about the scattering mechanism, polarimetric target decomposition methods have been evolved (Arai & Wang, 2007). As a result of extracting single, double and volume bounce scattering by target decompositions, different features such as city, road and forest can accurately be identified. In recent years, the accessibility of polarimetric SAR data has been growing owing to new satellite sensors such as UAVSAR, Sentinel-1 and ALOS-2 PALSAR-2. One of the major data sources of applications of Earth observation is Airborne SAR which is applied because of the privilege of not being reliant on meteorological conditions. Hence, SAR images are broadly employed in change detection applications such as damage assessment, crop monitoring, urban growth, etc. in order to perform multi-temporal analysis (Pirrone et al., 2016).

In 2012 and 2015 different techniques in change detection were analyzed for data fusion contests arranged by the IEEE Data Fusion Technical Committee (Berger et al., 2013), using various remote sensing data such as optical (Ahmed et al., 2016; Zhong et al., 2016), LiDAR (Zhang & Glennie, 2014), hyperspectral (Yang & Sun, 2015) and SAR data (Aghababae et al., 2012). Since, change detection using SAR images is more challenging than optical ones due to the existence of multiplicative speckle noise (Jia et al., 2015). It is crucial to obtain a robust SAR image change detection method which works properly despite the speckle noise. In contrast to the recent studies (Bazi et al., 2005; Bovolo & Bruzzone, 2005; Bazi et al., 2006; Carincotte et al., 2006; Ma et al., 2012; Gao et al., 2014; Hou et al., 2014) which the log-ratio operator is applied to the original SAR image, in this paper, due to the use of full polarimetric images, the coherency matrix (T), polarimetric decomposition, segmentation and data analysis features are extracted, and log ratio and difference operators are applied to the features. The use of decompositions increases the detection power due to extraction of single, double and volume bounce components. Since the log ratio operator is derived to be robust to calibration and radiometric errors, the log ratio operator is the most widely used method (Bazi et al., 2005; Gao et al., 2014; Hou et al., 2014). Therefore, it can somewhat reduce the effect of speckle noise. However, difference images are generated by the log ratio operator have noisy regions. The researchers (Gao et al., 2014; Hou et al., 2014; Zheng et al., 2014) proposed several improved log-ratio operators to solve the problem.

The pixels in DI (Difference Image) are classified into changed and unchanged classes. The reason for applying the DI classification step is to avoid the disadvantages of thresholding approaches. Several algorithms have been proposed for DI classification. For example, apply a reformulated fuzzy C means (FCM) clustering algorithm to

classify DI (Gong et al., 2012) or design a two-level clustering algorithm in order to discriminate changed and unchanged pixels (Li et al., 2015). The DI clustering methods can suppress the influence of speckle noise to a certain level. However, some information may be lost. further improvement can be achieved If more extracted features are utilized (Gao et al., 2016). In recent years, because of the increasing interest to the features of polarimetric channels, some works have been accomplished for CD (Change Detection) applications using PolSAR data (Borghys et al., 2007; Al-Sharif et al., 2013; Pirrone et al., 2016; Zhao et al., 2017). UAVSAR data is among appropriate data due to having full polarimetric channels and high spatial resolution. In these works, analysis focuses on the use of the likelihood ratio, analysis of features from polarimetric decompositions and stack of the log ratio based on features. The change detection is based on both the statistical model of different classes and unsupervised classification methods. In the classification step, the pixels in the log-ratio are classified into changed and unchanged classes.

The log-ratio operator is applied to the coherency matrix (T) and polarimetric decomposition, and also the log-ratio and difference operators are compared and fused. In the feature extraction step, the up-to-date and recent decompositions such as Unified Huynen (Li & Zhang, 2016) are implemented. In this paper, the Kernel K-means algorithm is applied. Kernel k-means is an extension of the standard k-means clustering algorithm that identifies nonlinearly separable clusters. The algorithm does not depend on cluster initialization, identifies nonlinearly separable clusters, and due to its incremental nature and search procedure, locates near optimal solutions by avoiding poor local minima. In order to different nature of the used operators, decision level fusion should be applied.

Based on this representation, we derive an unsupervised CD approach for the detection of different kinds of changes in the scene. This paper presents a change detection algorithm based on the log-ratio decomposition feature and classification DI, which is divided into four parts. Section 2.1 describes the pre-processing SAR data. Section 2.2 describes the extracting features using the coherency matrix (T), polarimetric decomposition, segmentation, and data analysis. Section 2.3 describes the DI generation by the log-ratio and difference operator. Section 2.4 describes the classification of the log-ratio feature using an unsupervised method.

2. The Proposed Method

After acquiring and pre-processing data, the coherency matrix (T), polarimetric decomposition, segmentation, and data analysis features are extracted. Then, the log-ratio and difference operators are applied to the features. After preparing DI, the unsupervised classification method, i.e.

kernel K-means, is employed to generate change maps. Figure 1 shows the main framework to generate change maps.

2.1. Data acquisition and preprocessing

UAVSAR data is L-band. L-band data are less affected by temporal decorrelation due to changes in the surface conditions over time. First, images are obtained at two different dates and then are preprocessed. The both images are ground-range detected (GRD), meaning that pre-processes such as radiometric calibration (conversion of intensity to surface reflectance) and multilooking along

with topographic correction are applied to the images. Thus, the images do not need geometric correction, and it is only required to reduce speckle noise in them.

The Refined Lee filter is specifically designed to preserve spatial resolution, it also minimize or even avoid mixture in scattering classes (Foucher & López Martínez, 2014). In addition, The Refined Lee approach improves the observation of the building edges so this filter is suitable choice as speckle filter. The both images are pre-processed using the Refined Lee filter (Yommy et al., 2015) to remove some speckle noise, and a number of images were co-registered by selecting proper GCPs (image to image).

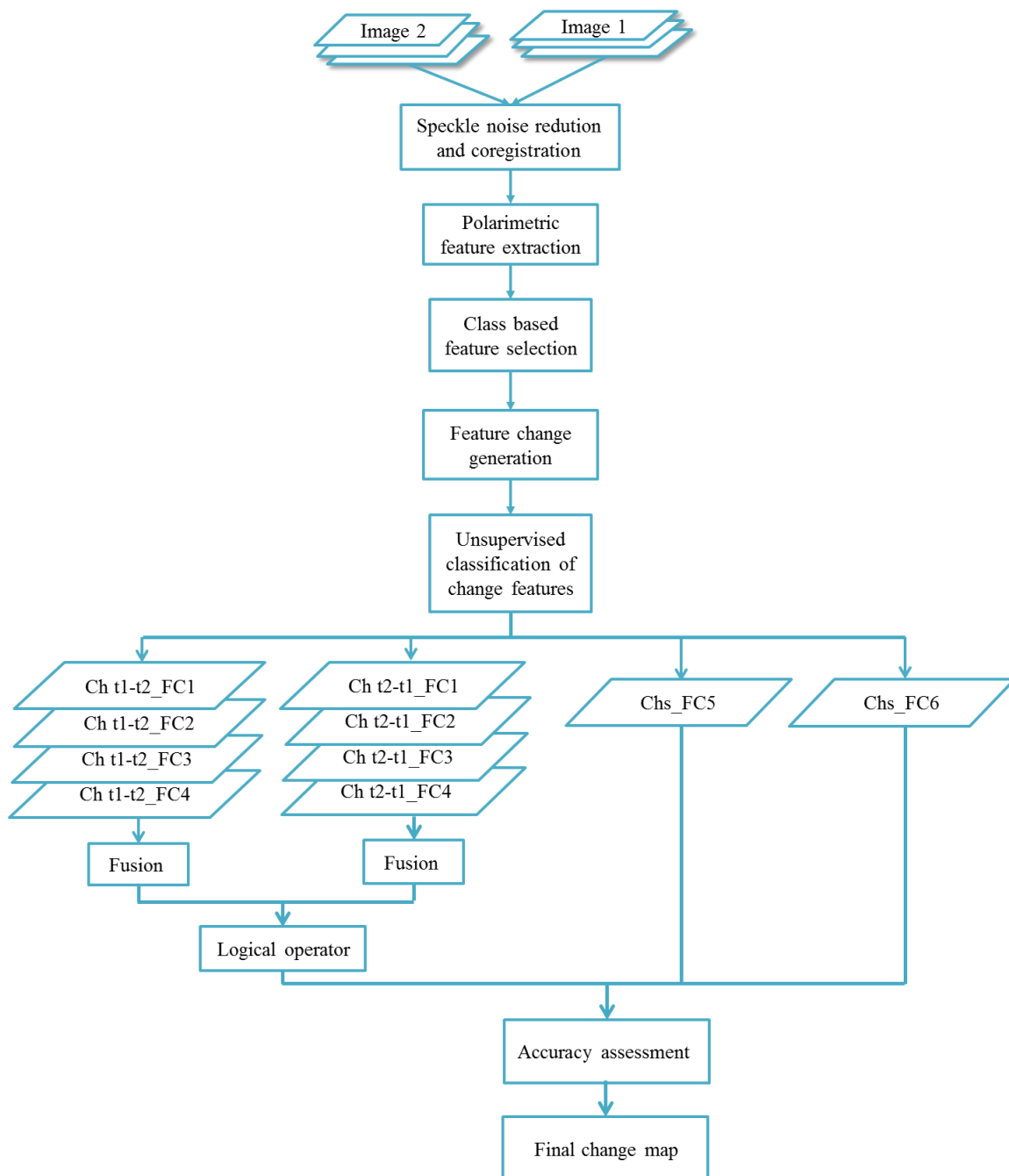


Figure 1. The proposed framework of the change detection algorithm

2.2. Feature extraction

In this study, in order to improve change detection, features are extracted using the coherency matrix (T), polarimetric decomposition, segmentation, and data analysis. Several methods are examined such as (a) decompositions: Singh (Singh et al., 2013), An & Yang (An et al., 2010), Freeman (Freeman & Durden, 1998), Yamaguchi (Yamaguchi et al., 2005), Krogager (Krogager, 1990), H/A/Alpha (Hajnsek et al., 2003), Unified Huynen (Li & Zhang, 2016), (b) segmentation: Wishart, H/A/Alpha (Ferro-Famil et al., 2001) and (c) data analysis: texture analysis (Kandaswamy et al., 2005).

To select appropriate features, a small area is selected and the proposed method is implemented on different decompositions. Then, the accuracy of the results is estimated with ground truth, and appropriate features are selected based on accuracy.

In accordance with the model-based decomposition technique, the decomposition of a target matrix into a mixture of physical scattering mechanisms, which corresponds to the surface (PS), double-bounce (PD), volume (PV), and helix scattering (PC) mechanisms is possible (Yamaguchi et al., 2005). This type of decomposition is based on simple scattering models that results in an easy-to-interpret scatter type discrimination.

2.2.1. The Singh four-component scattering power decomposition

In this method, the measured coherency matrix is rotated around the line of sight (Arii et al., 2011), and then to force $T_{23} = 0$ for different expressions of the scattering model, a unitary transformation is applied on the rotated coherency matrix. The steps and equations for calculating component

scattering are given below:

$$\langle [T] \rangle = \begin{bmatrix} T_{11} & T_{12} & T_{13} \\ T_{21} & T_{22} & T_{23} \\ T_{31} & T_{32} & T_{33} \end{bmatrix} = \frac{1}{n} \sum k_p k_p^\dagger \quad (1)$$

The Pauli vector k_p is defined as:

$$k_p = \frac{1}{\sqrt{2}} \begin{bmatrix} S_{HH} + S_{VV} \\ S_{HH} - S_{VV} \\ 2S_{HV} \end{bmatrix} \quad (2)$$

The rotation of around radar line of sight:

$$\langle [T(\theta)] \rangle = [R(\theta)] \langle [T] \rangle [R(\theta)]^\dagger \quad (3)$$

$$2\theta = \frac{1}{2} \tan^{-1} \left(\frac{2\text{Re}(T_{23})}{T_{22} - T_{33}} \right) \quad (4)$$

$$[R(\theta)] = \begin{bmatrix} 1 & 0 & 0 \\ 0 & \cos 2\theta & \sin 2\theta \\ 0 & -\sin 2\theta & \cos 2\theta \end{bmatrix} \quad (5)$$

Helix scattering power

$$P_c = 2[\text{Im}(T_{23})] \quad (6)$$

Volume scattering power

$$P_v = a[2T_{33}(\theta) - P_c] \quad (7)$$

The coefficient "a" is determined by the conditions.

Table 1 lists the Singh decomposition equations. The coefficient b is determined by the conditions.

After applying double unitary transformations, the T_{23} of the obtained rotated coherency matrix is completely removed. The Singh decomposition consists of seven parameters except the seven independent polarimetric parameters contained in the coherency matrix. It is found that the double bounce component is increased in urban areas (Singh et al., 2013).

Table 1. The Singh decomposition equations

In surface scattering dominant		In double bounce dominant	
$S = T_{11} - \frac{1}{2}P_v$	(8)	$S = T_{11}$	(13)
$D = TP - P_v - P_c - S$	(9)	$D = TP - P_v - P_c - S$	(14)
$C = T_{12}(\theta) + T_{13}(\theta) + bP_v$	(10)	$C = T_{12}(\theta) + T_{13}(\theta) + bP_v$	(15)
$P_s = S + \frac{ C ^2}{S}$ surface scattering	(11)	$P_d = D + \frac{ C ^2}{D}$ double bounce scattering	(16)
$P_d = D - \frac{ C ^2}{S}$ double bounce scattering	(12)	$P_s = S - \frac{ C ^2}{D}$ surface scattering	(17)

2.2.2. The An & Yang three-component model-based decomposition

Since the identity matrix can model pure volume scattering and be effective to decrease the volume scattering over urban areas, so this scattering matrix is appropriate for urban area decomposition. Comparing with freeman

decomposition, the An & Yang decomposition contains three extra steps. The first step before decomposition is the deorientation processing of the coherency matrix. The other two steps contain corresponding processes in order to prevent the emergence of negative powers. The steps and equations for calculating component scattering are given

below:

After calculating $[T(\theta)]$ using the Eq. (2), if $T_{11}(\theta) \leq T_{33}(\theta)$:

$$P_v = 3T_{11}(\theta), P_s = 0, P_d = T_{22}(\theta) + T_{33}(\theta) - 2T_{11}(\theta) \quad (18)$$

And if $T_{11}(\theta) \geq T_{33}(\theta)$:

$$P_v = 3T_{33}(\theta), x_{11} = T_{11}(\theta) - T_{33}(\theta), x_{22} = T_{22}(\theta) - T_{33}(\theta) \quad (19)$$

Table 2 lists the An & Yang decomposition equations.

Table 2. The An & Yang decomposition equations

$ T_{12}(\theta) ^2 > x_{11}x_{22}$		$ T_{12}(\theta) ^2 \leq x_{11}x_{22}$	
$x_{11} > x_{22}$	$x_{11} \leq x_{22}$	$x_{11} > x_{22}$	$x_{11} \leq x_{22}$
$P_s = x_{11} + x_{22}$	$P_s = 0$	$P_s = x_{11} + \frac{ T_{12}(\theta) ^2}{x_{11}}$	$P_s = x_{11} - \frac{ T_{12}(\theta) ^2}{x_{22}}$
$P_d = 0$	$P_d = x_{11} + x_{22}$	$P_d = x_{22} - \frac{ T_{12}(\theta) ^2}{x_{11}}$	$P_d = x_{22} + \frac{ T_{12}(\theta) ^2}{x_{22}}$

2.2.3. The Huynen decomposition

This decomposition introduces the SDoP for surface (SDoP_s), dihedral (SDoP_d), and volume scatterer (SDoP_v) as follows:

$$SDoP_s = \frac{\sum_{i=1}^3 |T_{i1}|^2}{T_{11} \sum_{i=1}^3 T_{ii}} \quad (20)$$

$$SDoP_d = \frac{\sum_{i=1}^3 |T_{i2}|^2}{T_{22} \sum_{i=1}^3 T_{ii}} \quad (21)$$

$$SDoP_v = \frac{\sum_{i=1}^3 |T_{i3}|^2}{T_{33} \sum_{i=1}^3 T_{ii}} \quad (22)$$

The three parameters can be quickly obtained because they directly relate to each column of T.

$$SDoP_3 = \frac{SDoP_s^2 + SDoP_d^2 + SDoP_v^2}{SDoP_s + SDoP_d + SDoP_v} \quad (23)$$

For single target the parameter SDoP₃ is 1, also for noisy target it is 1/3, and it resides between 1/3 and 1 for other targets. High SDoP₃ means a target has low randomness. Hence, it can measure target randomly.

The related research has demonstrated that there is no unique decomposition but rather infinity. Only when a certain aspect is preferred, Unique occur. Each decomposition cannot provide all information about target scattering but it has its own advantages. Therefore, for an united understanding of target decompositions, we need to

Adjacent urban and forested areas are clearly divided by applying the An & Yang method. Some areas sometimes show similar volume scattering characteristics such as these areas, and the outcome is not match with the real scattering mechanism. This method is consistent with both real scattering mechanisms and the physical meaning of power, because pixels with negative power are completely omitted (An et al., 2010).

merge all the decompositions (Li & Zhang, 2016).

2.3. Feature change generation

In this research, the log-ratio operator is applied to provide a difference image. Apart from making the changes well, the operator can reduce the influence of speckle noise. In addition to the log-ratio operator, the difference operator is also examined and in some cases provides acceptable results. Feature change images from the log-ratio operator are far better than those from the difference operator. At the end, the feature change images are selected with an appropriate accuracy, comparing to the ground truth image. A block scheme of the DI generation is depicted in Fig. 2.

A multi temporal comparison of the two PolSAR images is computed by defining a multi dimensional log ratio polarimetric feature image known as X_{LR}.

$$X_{LR} = [X_{LR, Singh}, X_{LR, An\&Yang}, X_{LR, SDoP}, \dots] \quad (24)$$

Here, X_{LR} has the same number of polarimetric features as input images, and it is defined as:

$$X_{LR} = \log \left(\frac{X_2}{X_1} \right) = \log X_2 - \log X_1 \quad (25)$$

Where X₁ and X₂ are the extracted features of the date 1 and date 2, respectively, and are defined as:

$$X_i = [X_{i, Singh}, X_{i, An\&Yang}, X_{i, SDoP}, \dots], i = 1, 2 \quad (26)$$

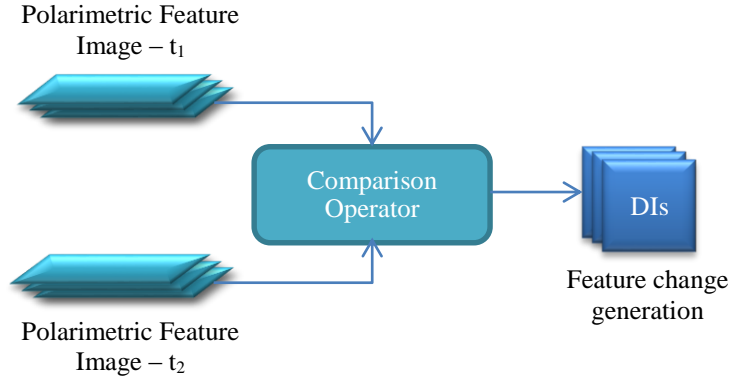


Figure 2. The block scheme of DI generation

2.4. Classification

By classifying the difference images, three classes are achieved: change t_1t_2 , change t_2t_1 and no-change. The defining of change t_1t_2 (changes from epoch1 to epoch2) is new objects that added to the area such as new buildings and also change t_2t_1 (changes from epoch2 to epoch1) means objects that removed from area such as destroyed buildings and deforestation.

In this paper, change detection is performed unsupervised, and thus unsupervised classification methods are used. Among the unsupervised classification methods, the kernel K-means method is applied in this study. The kernel k-means clustering algorithm applies the same method as k-means with the difference that in the calculation of distance, the kernel method is used instead of the Euclidean distance.

Compute the distance of each data point and the cluster center in the transformed space using:

$$D(\{\pi_c\}_{c=1}^k) = \sum_{c=1}^k \sum_{a_i \in \pi_c} \|\phi(a_i) - m_c\|^2 \quad (27)$$

where

$$m_c = \frac{\sum_{a_i \in \pi_c} \phi(a_i)}{|\pi_c|} \cdot \phi(a_i) \cdot \phi(a_i) - \frac{2 \sum_{a_j \in \pi_c} \phi(a_i) \phi(a_j)}{|\pi_c|} + \frac{\sum_{a_j, a_l \in \pi_c} \phi(a_j) \phi(a_l)}{|\pi_c|^2} \quad (28)$$

The c^{th} cluster is denoted by π_c .

' m_c ' denotes the mean of the cluster π_c .

' $\Phi(a_i)$ ' denotes the data point a_i in transformed space.

$\Phi(a_i) \cdot \Phi(a_j) = \exp(-\|a_i - a_j\|^q)$ for a Gaussian kernel.

$= (c + a_i \cdot a_j)^d$ for a polynomial kernel.

2.5. Fusion

The reason for fusing the produced change maps is to improve the results and reduce noise from radar data and change detection. To fuse the change maps, the majority voting and weighted majority voting algorithms are employed (i.e., weighing is performed using the accuracy of the results). Finally, to compare the results, the t_1t_2 and t_2t_1 change maps for each method are combined, and a change map is made for all changes.

Suppose that for a certain change detection problem, we have three different change maps $m_1(X)$, $m_2(X)$ and $m_3(X)$. We can combine these three maps in such a way as to produce a classifier that is superior to any of the individual maps. A common way to combine these maps is applying a majority voting algorithm.

$$C(X) = \text{mode}\{m_1(X), m_2(X), m_3(X)\} \quad (29)$$

In other words, at each value, X is classified to the change class that receives the largest number of votes (James, 1998).

3. Dataset Description

For a preliminary validation of the proposed CD strategy, we investigate a dataset from Oakland in California, as indicated in Fig. 3. between the period 2010 to 2017, the region was affected by urban expansion, deforestation and changing land use. We consider the pair of SAR data acquired by the UAVSAR satellite mission over the region in 2010 and 2017, respectively, as the input dataset. The both images contain a spatial resolution of 6.2m and full polarimetric channels (i.e., VV, HH, HV and VH). Table 3 lists the data specification such as acquisition date (before and after changes), band, polarization and spatial resolution.

Table 3. SAR Data specification

Sensor	Acquisition date (before changes)	Acquisition date (after changes)	Band	Spatial resolution (m)
UAVSAR	23/04/2010	03/04/2017	L-Band (Fully polarimetric)	6.2 x 6.2 (GRD)

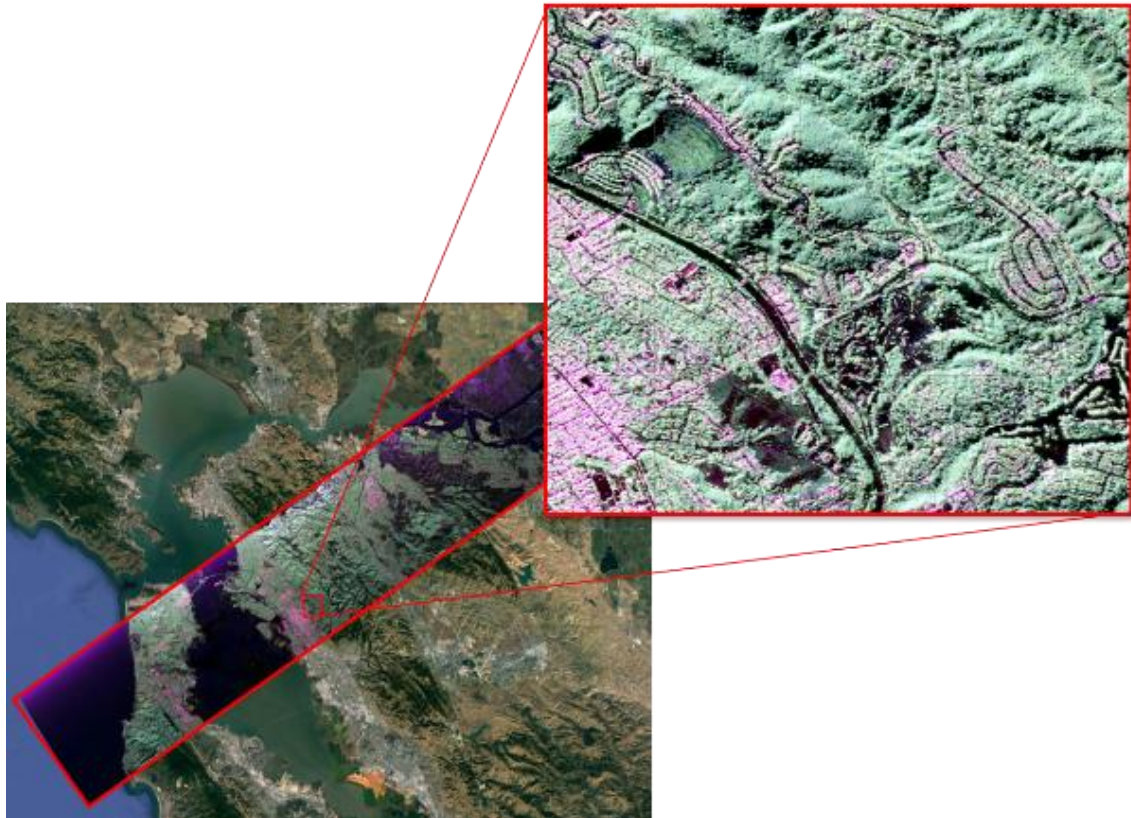


Figure 3. The case study

Table 4. Google Earth images specification

Dataset	Acquisition date (before changes)	Acquisition date (after changes)	Band	Spatial resolution (m)
QuickBird	06/06/2010	12/03/2017	R, G, B	0.75 × 0.6

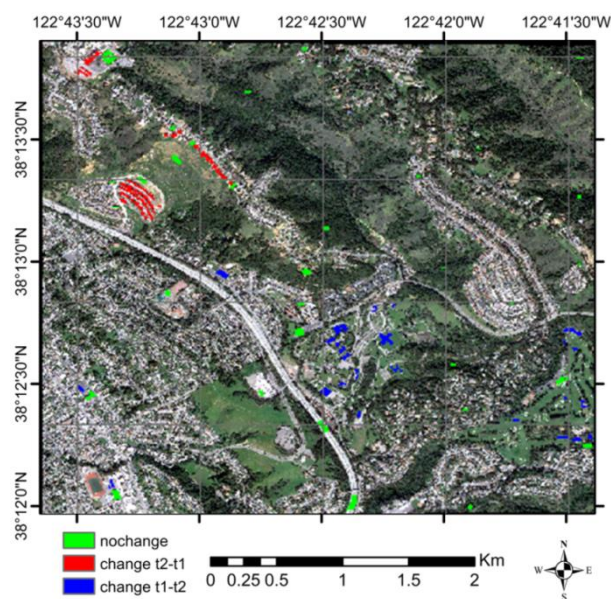


Figure 4. Ground truth

As the reference data, we consider Google Earth images as ground truth as well as training and testing data, representing the change map of the region between the period 2010 to 2017 (cf. Fig. 4). Table 4 lists the images specification such as acquisition date (before and after changes), band and spatial resolution.

4. Experimental Results

After preprocessing the data, the Pauli target decomposition is used to better represent the image.

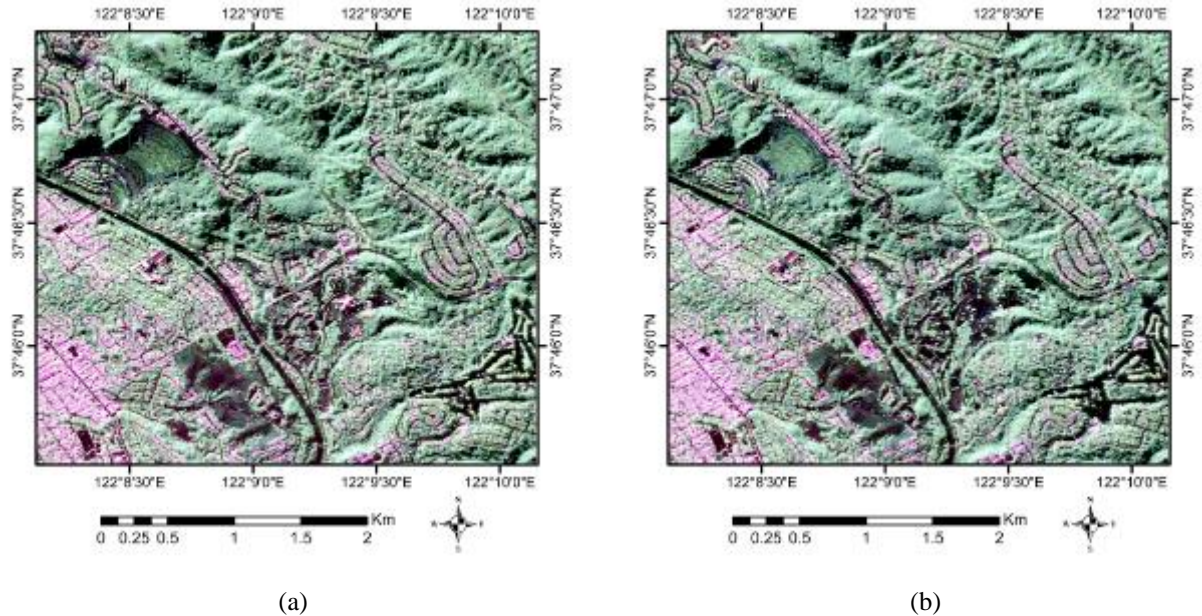


Figure 5. Color composition (Pauli RGB) for the years (a) 2010 and (b) 2017

By preparing different feature descriptors and evaluating them, the features that show different variations and coverages are selected. The selected features distinguish the ground cover better than the other features, e.g., the Cloude decomposition feature distinguishes urban areas well in comparison to the other land covers such as tree plants. The

selected features at this step are Cloude, Singh, An & Yang, $H / u / v$ classification, Unified Huynen classification, coherence matrix, and some texture features (including Dissimilarity, Homogeneity, Contrast, Entropy, Uniformity, Direction) . Figure 6 shows the selected features.

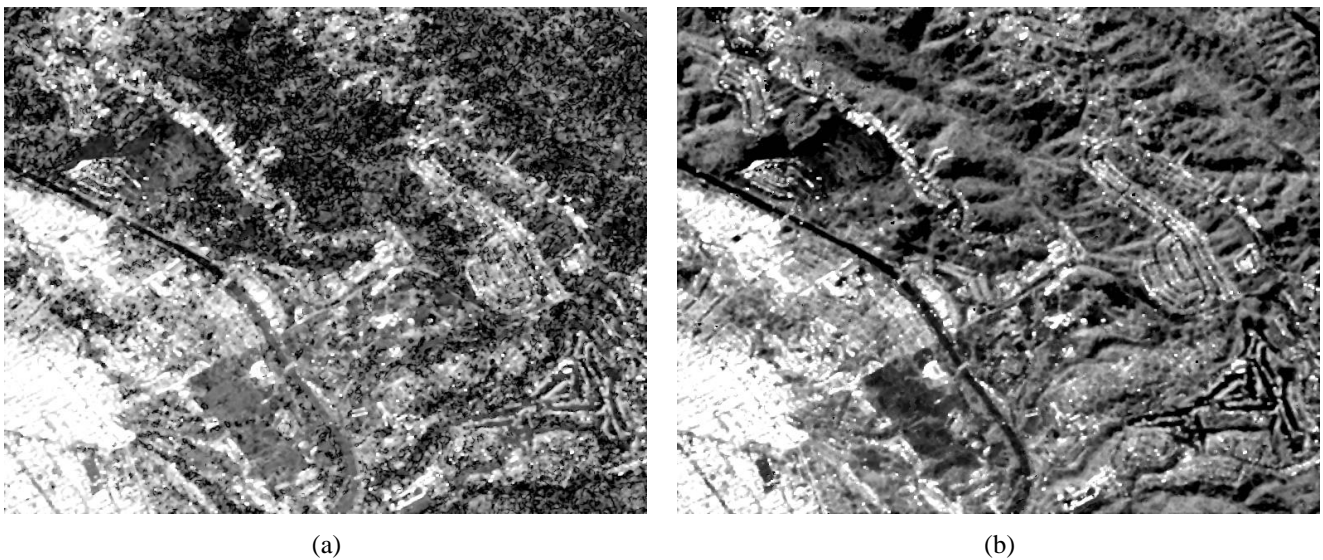
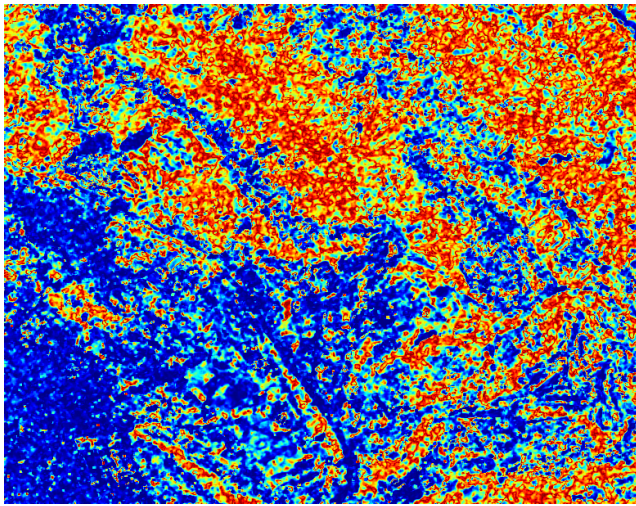


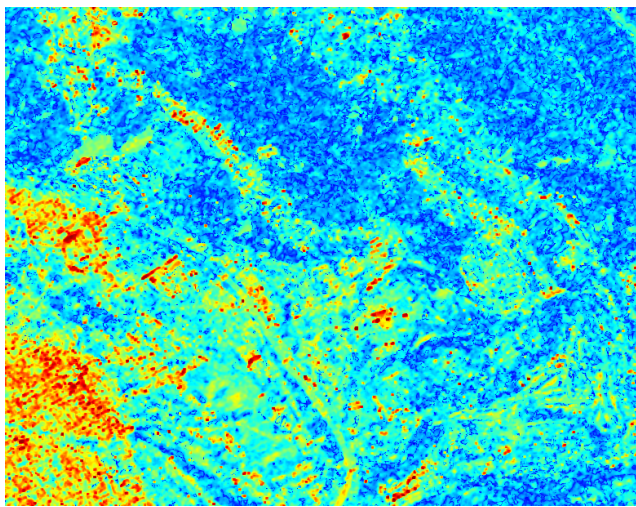
Figure 6. The selected features: Cloude (a), Singh (b), $H / u / v$ classification (c), An & Yang (d), Unified Huynen classification (e), Dissimilarity of T33 (f), Dissimilarity of T22 (g), Pauli RGB of the coherence matrix (h)



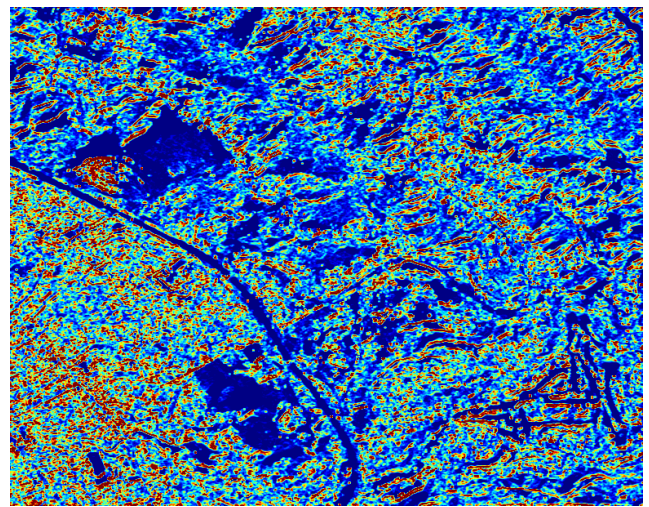
(c)



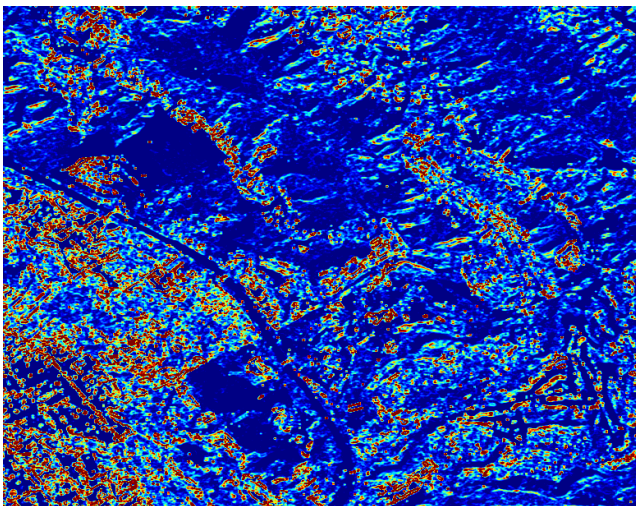
(d)



(e)



(f)



(g)



(h)

Figure 6. Continued.

In decompositions such as Cloude and $H / u / v$ classification, urban areas can be identified with more accuracy. High-rise and low-rise building compartments as

well as city green spaces can be extracted. In fact, low-density building areas can be distinguished by vegetation.

After selecting appropriate features, two operators, i.e.

log-ratio and difference, are used to generate DI. The results of the log-ratio operator show the changes much better. In the log-ratio operator, the feature ratios for both 2010 to 2017 and 2017 to 2010 period show changes from both 2010 to 2017 and 2017 to 2010, respectively. The best DIs are related to the application of the log-ratio operator on Singh, An & Yang, Unified Huynen classification and coherency matrices.

The selected DIs are stacked together and used as inputs to the classification method. The classification methods of kernel K-means are employed to classify the DIs. Different stacks of the DIs are used as inputs for the classification methods. The results are named as "the group of changes feature combination". Table 5 lists the utilized feature combinations.

The two groups of changes are considered as: $Ch_{t_1t_2}$ as changes from 2010 to 2017 and $Ch_{t_2t_1}$ as changes from 2017 to 2010. A change map depends on the classification input DIs to detect both the "change t_1t_2 " and "change t_2t_1 " classes. Because of the mathematical basis of the logarithm, when the ratio value in front of the log is zero, the log-ratio value will be $-\text{INF}$. Therefore, for decompositions, both $\frac{t_1}{t_2}$ and $\frac{t_2}{t_1}$ are separately calculated due to the pixels with near zero values and $-\text{INF}$ for the log ratio. While the coherency matrix has close values, the ratio of the two dates is not

zero. Thus, by using only one ratio, the both groups of changes can be extracted. Results for change maps are indicated in Fig. 7.

Table 1. Feature combination

Feature Combination	Stacked DIs
FC1	Singh_Dbl, An&Yang_Dbl, SDoPd_R, SDoPd_B
FC2	Singh_Dbl, An&Yang_Dbl, SDoPd_B
FC3	Singh_Dbl, An&Yang_Dbl
FC4	T11(Using log-ratio and difference)
FC5	T11,T22,T33
FC6	T11,T22,T33 (Using log-ratio and difference)

The three maps (a), (c), and (e) of the t_2t_1 group, which show better accuracy (as shown in charts) than other maps, are fused. Moreover, the three maps (b), (d), and (f) of the t_1t_2 group are fused. Then, the fusion results are combined and the final change map is obtained. This process is performed for the majority voting and weighted majority voting algorithms. The two FC4 maps with the highest accuracy are also combined. Results are indicated in Fig. 8.

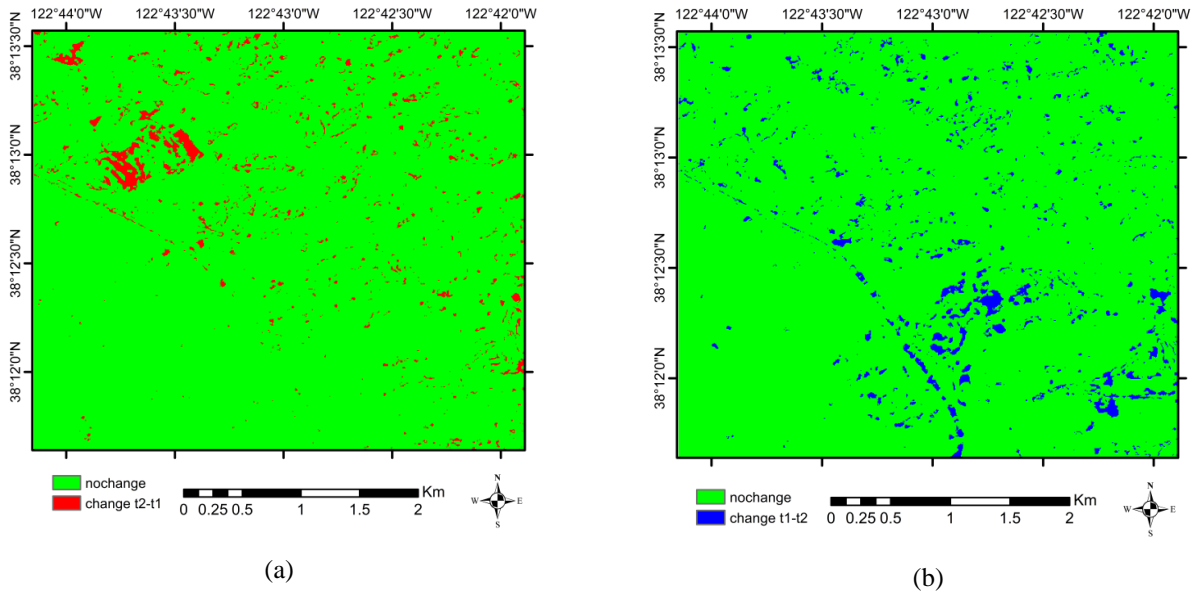
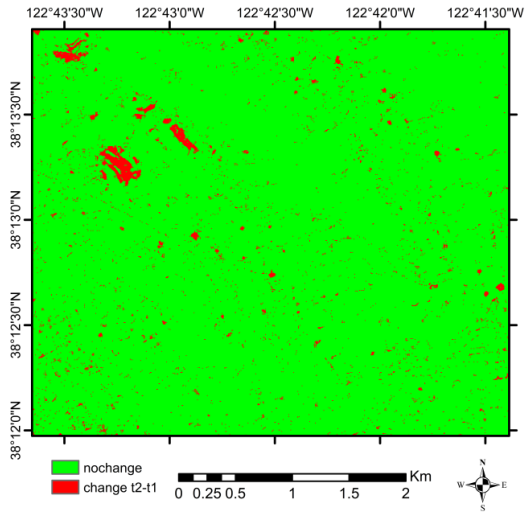
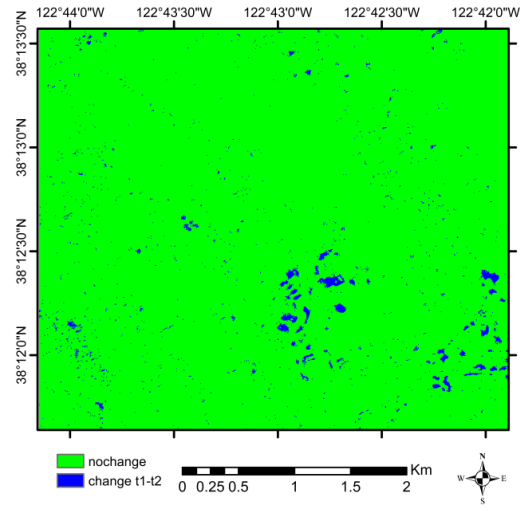


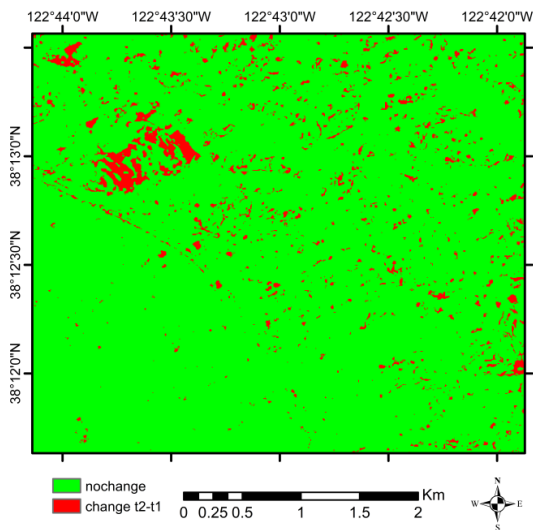
Figure 7. Change maps: $Ch_{t_2t_1}$ -FC3 (a), $Ch_{t_1t_2}$ -FC3 (b), $Ch_{t_2t_1}$ -FC4 (c), $Ch_{t_1t_2}$ -FC4 (d), $Ch_{t_2t_1}$ -FC2 (e), $Ch_{t_1t_2}$ -FC2 (f), Chs_FC5 (g), Chs_FC6 (h)



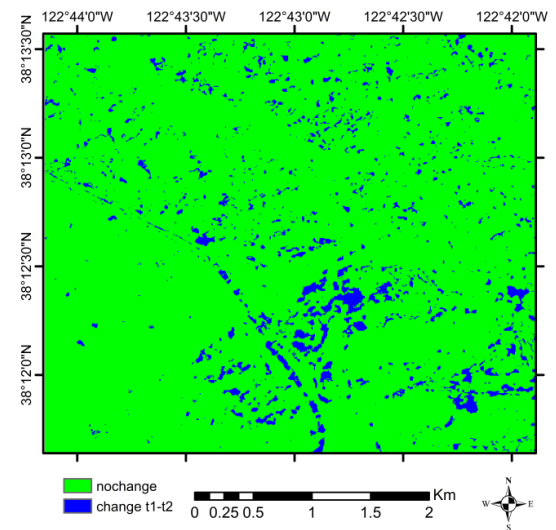
(c)



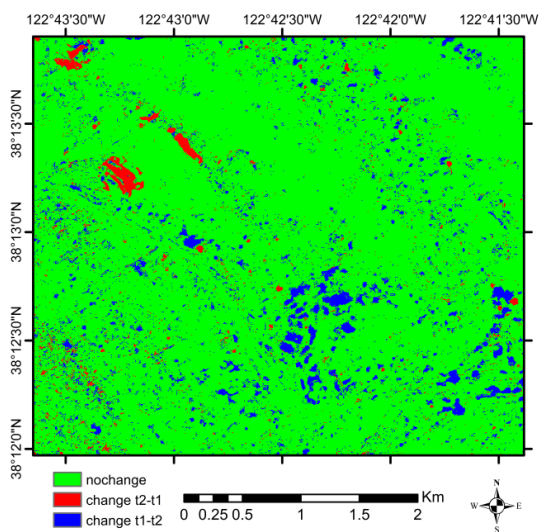
(d)



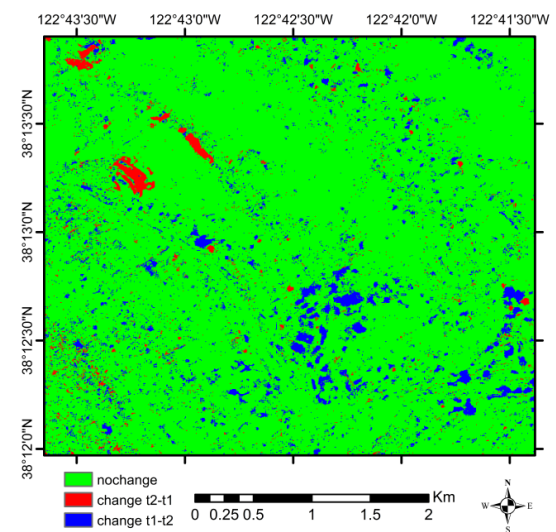
(e)



(f)



(g)



(h)

Figure 7. Continued.

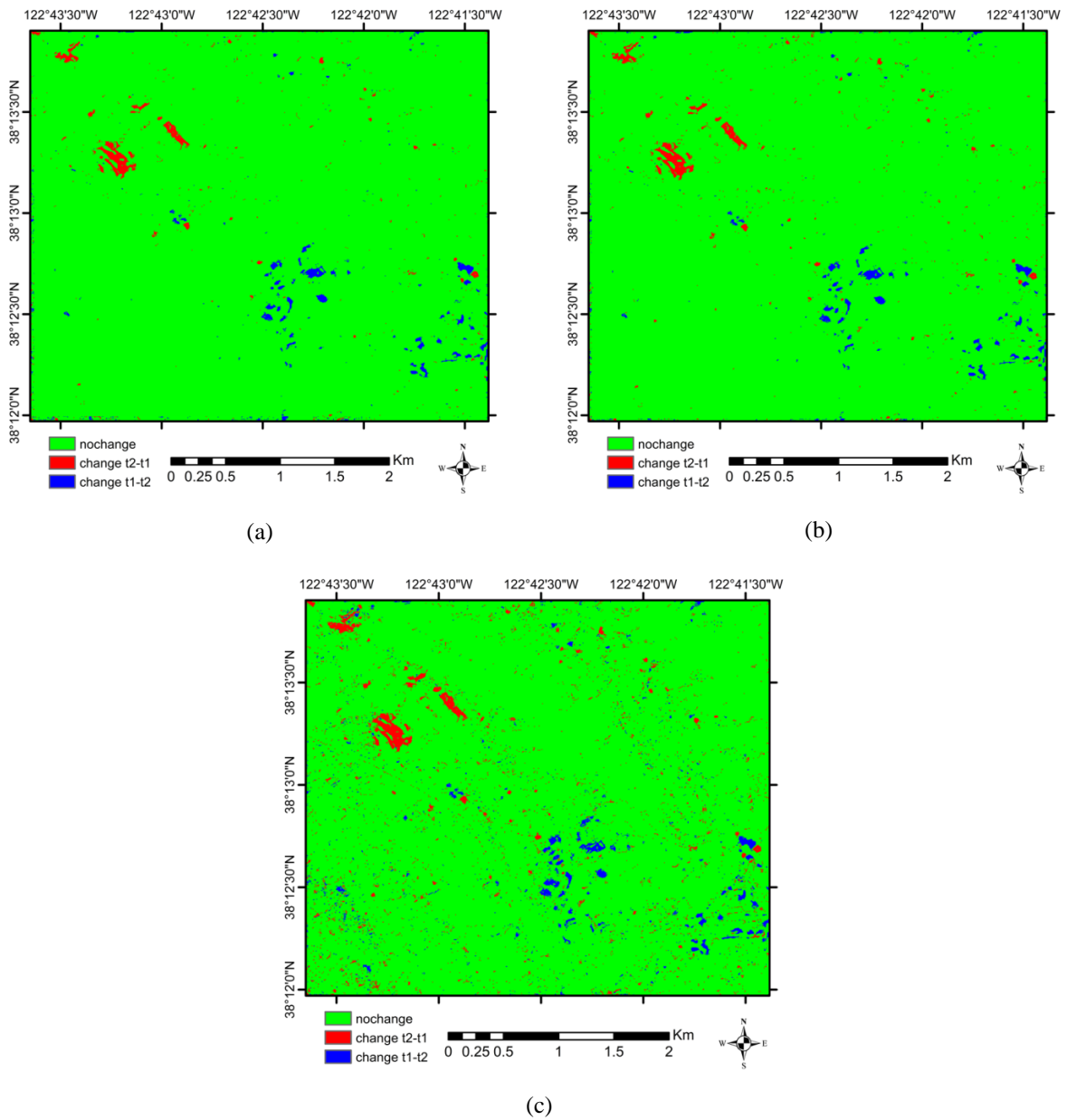


Figure 8. Change maps: AND_MV (a), AND_WMV (b), AND_FC4 (c)

By comparing the fused change map and the change maps developed in the previous step, noise reduction in the fused map can be observed (Fig. 8).

The results are evaluated using ground truth from Google Earth images with two criteria: overall accuracy (OA) and Kappa coefficients. The evaluation of the final results of change t_1t_2 and t_2t_1 can be observed in Tables. 6 and 7, respectively. Accordingly, the best accuracy is related to the change map " $Ch_{t_1t_2_FC4}$ " with an overall accuracy of 87.58% and Kappa of 0.7407 for $Ch_{t_1t_2}$ and also for the change map " $Ch_{t_2t_1_FC4}$ " with an overall accuracy of

87.74% and Kappa of 0.7457 for $Ch_{t_2t_1}$.

Table 6. Evaluation of the change t_1t_2 results

Change results	Overall Accuracy	Kappa
$Ch_{t_1t_2_FC1}$	70.16	54.8
$Ch_{t_1t_2_FC2}$	73.12	59.28
$Ch_{t_1t_2_FC3}$	85.65	70.92
$Ch_{t_1t_2_FC4}$	87.58	74.07

Table 7. Evaluation of the change t_2t_1 results

Change results	Overall Accuracy	Kappa
Cht t_1 _FC1	77.3	51.21
Cht t_1 _FC2	80.28	65.32
Cht t_1 _FC3	86.35	71.69
Cht t_1 _FC4	87.74	74.57

The evaluation of the final results of changes can be observed in Table 8. As indicated, fusion with the MV and WMV algorithms does not improve the results, but the weighting algorithm yields better results as compared to the unweighted algorithm. The FC4 combined map shows a good result, but FC5 and FC6 are more accurate due to the use of the three features T11, T22 and T33. Further, FC6 achieves the best result due to the use of both the difference and log-ratio operators. According to the chart, the best accuracy is related to the change map of "Chs_FC6" with an overall accuracy of 86.27% and Kappa of 0.7922 for the both groups.

Table 8. Evaluation of the changes results

Change results	Overall Accuracy	Kappa
Chs_FC5	84.89	77.27
Chs_FC6	86.27	79.22
AND_MV	77.96	65.72
AND_WMV	79.03	67.45
AND_FC4	81.88	72.21

As shown in the charts, the log-ratio operator has far better results in comparison to the difference operator. However, the optimum option is the simultaneous use of both the operators so that the noise and error of the log-ratio operator can be reduced using the difference operator. According to the final results, it can be concluded that the coherence matrix is a better feature for detecting changes than other features.

5. Conclusions

The world intends to carry out projects without human intervention and we seek to research and advance knowledge in this area. Therefore supervised methods may be more accurate; but we attempt to improve unsupervised methods. In this paper, we proposed an unsupervised change detection approach for SAR image pairs. Our proposed algorithm can be divided into the following main

steps: (1) we used several method to provide features using the coherency matrix (T), polarimetric decomposition, segmentation and data analysis; (2) we use the two different operators of log-ratio and difference to produce difference images; (3) we apply two unsupervised classification methods to obtain final change maps; (4) we apply a majority voting algorithm to fuse change maps and combine the t_1t_2 and t_2t_1 change maps.

The existing SAR image change detection methods first generate a DI and then use clustering methods to classify the pixels of the DI into changed and unchanged classes. Using the proposed features to provide more accurate DI and ultimately achieving more accurate change maps will result in the superiority of the proposed algorithm.

Since the reference (Pirrone et al., 2016) uses only intensity as a log-ratio input, scattering mechanisms that have an effective role in identifying different coverings cannot be used and thus less change classes can be identified. Due to the use of the polarimetric feature, the probability of change detection error is reduced in the proposed method. Additionally, by using the difference operator, the noise of the change map is reduced.

In the presented automatic multi-class CD strategy, FC4 achieves the best result with an overall accuracy of 87% and Kappa of 74% in the both groups of changes, i.e. t_1t_2 and t_2t_1 . Considering all changes (both t_1t_2 and t_2t_1), FC6 yields the best results with an overall accuracy of 86% and Kappa of 79%.

The log-ratio operator shows far better results than the difference operator. However, the best option is to use both the operators simultaneously so the noise and error of the log-ratio operator can be reduced using the difference operator. According to the final results, it can be concluded that the coherence matrix is a better feature for detecting changes, as compared to other features.

According to experimental results, the false detection rate decreases and the accuracy of change detection is improved in this suggested algorithm. In addition, the investigation of the proposed method will be continued to discover the expansion of urban regions over time. Likewise, in our future research work, the fusion of optics and SAR data will be used to provide better results in identifying different coverings and detecting changes. We will also seek to distinguish the physical meaning of changes and organize the "from-to" map.

References

- Aghababae, H., Tzeng, Y.-C. & Amini, J. (2012). "Swarm intelligence and fractals in dual-pol synthetic aperture radar image change detection." *Journal of Applied Remote Sensing* 6(1): 063596.
- Ahmed, T., Singh, D. P. & Raman, B. (2016). "Potential application of Kanade–Lucas–Tomasi tracker on

- satellite images for automatic change detection." *Journal of Applied Remote Sensing* **10**(2): 026018.
- Al-Sharif, A. A., Pradhan, B., Hadi, S. J. & Mola, N. (2013). Revisiting methods and potentials of sar change detection. *Proceedings of the World Congress on Engineering*.
- An, W., Cui, Y. & Yang, J. (2010). "Three-component model-based decomposition for polarimetric SAR data." *IEEE Transactions on Geoscience and Remote Sensing* **48**(6): 2732-2739.
- Arai, K. & Wang, J. (2007). "Polarimetric SAR image classification with the maximum curvature of the trajectory in the eigen space converted from the polarization signature." *Advances in Space Research* **39**(1): 149-154.
- Arii, M., van Zyl, J. J. & Kim, Y. (2011). "Adaptive model-based decomposition of polarimetric SAR covariance matrices." *IEEE Transactions on Geoscience and Remote Sensing* **49**(3): 1104-1113.
- Bazi, Y., Bruzzone, L. & Melgani, F. (2005). "An unsupervised approach based on the generalized Gaussian model to automatic change detection in multitemporal SAR images." *IEEE Transactions on Geoscience and Remote Sensing* **43**(4): 874-887.
- Bazi, Y., Bruzzone, L. & Melgani, F. (2006). "Automatic identification of the number and values of decision thresholds in the log-ratio image for change detection in SAR images." *IEEE Geoscience and Remote Sensing Letters* **3**(3): 349-353.
- Berger, C., Voltersen, M., Eckardt, R., Eberle, J., Heyer, T., Salepci, N., Hese, S., Schmullius, C., Tao, J. & Auer, S. (2013). "Multi-modal and multi-temporal data fusion: Outcome of the 2012 GRSS data fusion contest." *IEEE Journal of Selected Topics in Applied Earth Observations and Remote Sensing* **6**(3): 1324-1340.
- Borghys, D., Shimoni, M. & Perneel, C. (2007). Change detection in urban scenes by fusion of SAR and hyperspectral data. *Remote Sensing for Environmental Monitoring, GIS Applications, and Geology VII*, International Society for Optics and Photonics.
- Bovolo, F. & Bruzzone, L. (2005). "A detail-preserving scale-driven approach to change detection in multitemporal SAR images." *IEEE Transactions on Geoscience and Remote Sensing* **43**(12): 2963-2972.
- Carincotte, C., Derrode, S. & Bourennane, S. (2006). "Unsupervised change detection on SAR images using fuzzy hidden Markov chains." *IEEE Transactions on Geoscience and Remote Sensing* **44**(2): 432-441.
- Ferro-Famil, L., Pottier, E. & Lee, J.-S. (2001). "Unsupervised classification of multifrequency and fully polarimetric SAR images based on the H/A/Alpha-Wishart classifier." *IEEE Transactions on Geoscience and Remote Sensing* **39**(11): 2332-2342.
- Foucher, S. & López-Martínez, C. (2014). "Analysis, evaluation, and comparison of polarimetric SAR speckle filtering techniques." *IEEE transactions on image processing* **23**(4): 1751-1764.
- Freeman, A. & Durden, S. L. (1998). "A three-component scattering model for polarimetric SAR data." *IEEE Transactions on Geoscience and Remote Sensing* **36**(3): 963-973.
- Gao, F., Dong, J., Li, B., Xu, Q. & Xie, C. (2016). "Change detection from synthetic aperture radar images based on neighborhood-based ratio and extreme learning machine." *Journal of Applied Remote Sensing* **10**(4): 046019.
- Gao, G., Wang, X., Niu, M. & Zhou, S. (2014). "Modified log-ratio operator for change detection of synthetic aperture radar targets in forest concealment." *Journal of Applied Remote Sensing* **8**(1): 083583.
- Gong, M., Zhou, Z. & Ma, J. (2012). "Change detection in synthetic aperture radar images based on image fusion and fuzzy clustering." *IEEE Transactions on Image Processing* **21**(4): 2141-2151.
- Hajnsek, I., Pottier, E. & Cloude, S. R. (2003). "Inversion of surface parameters from polarimetric SAR." *IEEE Transactions on Geoscience and Remote Sensing* **41**(4): 727-744.
- Hou, B., Wei, Q., Zheng, Y. & Wang, S. (2014). "Unsupervised change detection in SAR image based on Gauss-log ratio image fusion and compressed projection." *IEEE J. Sel. Top. Appl. Earth Obs. Remote Sens* **7**(8): 3297-3317.
- James, G. (1998). Majority vote classifiers: theory and applications, Stanford University.
- Jia, L., Li, M., Wu, Y., Zhang, P., Liu, G., Chen, H. & An, L. (2015). "SAR image change detection based on iterative label-information composite kernel supervised by anisotropic texture." *IEEE Transactions on Geoscience and Remote Sensing* **53**(7): 3960-3973.
- Kandaswamy, U., Adjeroh, D. A. & Lee, M.-C. (2005). "Efficient texture analysis of SAR imagery." *IEEE Transactions on Geoscience and Remote Sensing* **43**(9): 2075-2083.
- Krogager, E. (1990). "New decomposition of the radar target scattering matrix." *Electronics Letters* **26**(18): 1525-1527.
- Li, D. & Zhang, Y. (2016). "Unified Huynen phenomenological decomposition of radar targets and its classification applications." *IEEE Transactions on Geoscience and Remote Sensing* **54**(2): 723-743.
- Li, H.-C., Celik, T., Longbotham, N. & Emery, W. J. (2015). "Gabor feature based unsupervised change detection of multitemporal SAR images based on two-level clustering." *IEEE Geoscience and Remote Sensing Letters* **12**(12): 2458-2462.

- Ma, J., Gong, M. & Zhou, Z. (2012). "Wavelet fusion on ratio images for change detection in SAR images." *IEEE Geoscience and Remote Sensing Letters* **9**(6): 1122-1126.
- Pirrone, D., Bovolo, F. & Bruzzone, L. (2016). A novel framework for change detection in bi-temporal polarimetric SAR images. *Image and Signal Processing for Remote Sensing XXII*, International Society for Optics and Photonics.
- Schmitt, A. & Brisco, B. (2013). "Wetland monitoring using the curvelet-based change detection method on polarimetric SAR imagery." *Water* **5**(3): 1036-1051.
- Sharma, S. & Mathur, P. (2004). "Change detection analysis of avalanche snow in Himalayan region using near infrared and active microwave images." *Advances in Space Research* **33**(3): 259-267.
- Singh, G., Yamaguchi, Y. & Park, S.-E. (2013). "General four-component scattering power decomposition with unitary transformation of coherency matrix." *IEEE Transactions on Geoscience and Remote Sensing* **51**(5): 3014-3022.
- Ulaby, F. T., Moore, R. K. & Fung, A. K. (1986). "Microwave remote sensing active and passive-volume III: from theory to applications."
- Yamaguchi, Y., Moriyama, T., Ishido, M. & Yamada, H. (2005). "Four-component scattering model for polarimetric SAR image decomposition." *IEEE Transactions on Geoscience and Remote Sensing* **43**(8): 1699-1706.
- Yang, J. & Sun, W. (2015). "Automatic analysis of the slight change image for unsupervised change detection." *Journal of Applied Remote Sensing* **9**(1): 095995.
- Yommy, A. S., Liu, R. & Wu, S. (2015). SAR image despeckling using refined Lee filter. *Intelligent Human-Machine Systems and Cybernetics (IHMSC), 2015 7th International Conference on*, IEEE.
- Zhang, X. & Glennie, C. (2014). Change detection from differential airborne LiDAR using a weighted anisotropic iterative closest point algorithm. *Geoscience and Remote Sensing Symposium (IGARSS), 2014 IEEE International*, IEEE.
- Zhao, J., Yang, J., Lu, Z., Li, P., Liu, W. & Yang, L. (2017). "A novel method of change detection in bi-temporal polSAR data using a joint-classification classifier based on a similarity measure." *Remote Sensing* **9**(8): 846.
- Zheng, Y., Zhang, X., Hou, B. & Liu, G. (2014). "Using Combined Difference Image and k -Means Clustering for SAR Image Change Detection." *IEEE Geoscience and Remote Sensing Letters* **11**(3): 691-695.
- Zhong, C., Xu, Q. & Li, B. (2016). "Relative radiometric normalization for multitemporal remote sensing images by hierarchical regression." *IEEE Geoscience and Remote Sensing Letters* **13**(2): 217-221.